RSC Advances

ROYAL SOCIETY OF CHEMISTRY

www.rsc.org/advances

RSC Advances

RSCPublishing

PAPER

Modulation of human mesenchymal stem cell survival on electrospun mesh with co-immobilized epithelial growth factor and gelatin

Cite this: DOI: 10.1039/xoxxoooooox

Received ooth January 2012,
Accepted ooth January 2012

DOI: 10.1039/xoxxoooooox

www.rsc.org/

Young Min Shin,[§a] Jong-Young Lim,[§a] Jong-Seok Park,[a] Hui-Jeong Gwon,[a] Sung In Jeong,[a] Sung-Jun An,[a] Heungsoo Shin,[b] and Youn-Mook Lim*[a]

In this work, we present a biomimetic fibrous scaffold containing two biomolecules. Biocompatible poly (L-lactide-co-ε-caprolactone) mesh was fabricated by an electrospinning method, and then acrylic acid was grafted on the mesh to introduce a carboxyl group through γ-ray irradiation. Subsequently, epidermal growth factor (EGF) and gelatin were coupled to the mesh through EDC reaction. The modified mesh presents a consistent fibre diameter (874.4 ± 178.5 nm), having carboxyl groups (1.3 mM). EGF (171.7 ng mg^{-1}mesh) and gelatin (67.2 ± 30.5 μg mg^{-1} mesh) were successfully coupled on the mesh. The coupled EGF and gelatin promoted the cell viability 1.5-times higher than that from non-modified mesh. In particular, the EGF on the meshes independently allowed hMSC present 3-times greater involucrin expression and enabled improved procollagen secretion, implying trans-differentiation of hMSC to keratinocyte-like cells. Therefore, the co-immobilization strategy of biomolecules using radiation technology may be an alternative tool for tissue engineering applications.

1. Introduction

In tissue engineering, a biomimetic strategy has attracted great interest due to potential for fabricating the artificial construct of a native tissues or organs.[1] Conventionally, tissue engineering scaffolds have been designed to have a porous structure that can allow cell adhesion and proliferation.[2] The fabrication of these scaffolds was conducted by salt-leaching or gas-forming methods, generating interconnected pores with a few hundred microns.[3,4] However, an advanced investigation for ideal scaffolds has focused on the structure and function of an extracellular matrix (ECM) in native tissue, and the structural difference between conventional scaffolds and ECM has been magnified in the field.[5] ECM consists of a variety of proteins and proteoglycans, in which the cell binds to the collagen fibrils presenting a mature cytoskeleton formation or transferring an intrinsic signal for regulating the cellular behaviours.[6] However, porous scaffolds do not have such fibrous architectures, which has been recently achieved by an electrospinning method. Electrospinning has been introduced as an alternative method for generating ECM-like nanofibrous scaffolds with higher porosity and three-dimensional fibrous structure.[7] Most of the polymers including synthetic polymers or natural polymers have been utilized to generate the nanofibres for tissue engineering scaffolds.[8-12]

Although an ECM-like artificial construct for tissue regeneration has been successfully fabricated by electrospinning methods, their ability to improve the cell viability was partially advanced by topological cues.[13] In addition, the fundamental biological property has not been fully addressed. Recently, a biological property of ECM has been guaranteed through biomimetic modification.[14] The core strategy has focused on biomolecule conjugation via a general surface modification. For example, acrylic acid (AAc) grafted nanofiber via plasma-exposure was coupled with collagen,[15] and Arginine-Glycine-Aspartic acid (RGD) peptide or growth factors such as the fibroblast growth factor-basic (FGF-basic) or vascular endothelial cell growth factor (VEGF) modified scaffolds effectively improved the proliferation and differentiation of the cells.[16,17] Furthermore, an alternative model for co-immobilization of biomolecules was reported, in which each molecule successfully played its own fundamental role in regulating the cell behaviors.[18] Indeed, because most of the biological cell responses have been harmonized by various proteins or biomolecules having different functions, a multi-molecule conjugation can expand the scaffold function for triggering target-specific tissue regeneration. Previously, Lee et al. reported that co-immobilized RGD peptide and FGF-basic via polydopamine coating could promote the behaviours of a human umbilical cord vein endothelial cells (HUVEC)

including proliferation, migration, and protein expression.[19] A gradient-pattern with EGF and insulin-like growth factor-I (IGF-I) was prepared by photo-reactive coupling reaction, and controlled migration speed of keratinocytes.[20] However, there is no nanofibre co-immobilized with biomolecules, and we did not find an approach for an artificial construct having an ECM-like microstructure and biological property.

For this report, we developed a biofunctional nanofibrous mesh co-immobilized with two individual biomolecules using radiation technology for tissue engineering. Based on the electrospun meshes, we coupled the epidermal growth factor (EGF) and gelatin to construct the biological features of the ECM as critical candidates for tissue regeneration. EGF is known as an essential growth factor to induce cell proliferation and skin tissue healing. In particular, it regulates the differentiation of stem cells to mature keratinocytes. Gelatin is derived from collagen through acid or base treatment, which has been used in the food and pharmaceutical industries owing to an easy production and cheap price. It is frequently utilized to fabricate the scaffolds or improve the biological property of synthetic material-based scaffolds owing to the similar function with collagen. We then investigated the effect of co-immobilized factors on the regulation of human mesenchymal stem cell (hMSC) behaviours, including adhesion and viability. Furthermore, we also examined whether the co-immobilized factors affect the differentiation of hMSC. Schematic diagram and illustration for hMSC adhesion on the modified mesh was presented in Fig. 1.

2. Experimental

2.1. Materials

2,2,2-trifluoroethanol (TFE), toluidine blue O, fluorescamine, acrylic acid (AAc), gelatin type B from bovine skin, ethyl(dimethylaminopropyl) carbodiimide (EDC), N-hydroxysuccinimide (NHS) and 2-(N-morpholino) ethanesulfonic acid sodium salt (MES) were purchased from Sigma-Aldrich (St. Louis, MO, USA). NaOH, HCl and dichloromethane (DCM) were purchased from Showa chemical (Tokyo, Japan). Dulbecco's phosphate buffered saline (DPBS), Dulbecco's modified eagle's medium (DMEM), foetal bovine serum (FBS), penicillin, and streptomycin were obtained from GIBCO (Carlsbad, CA, USA). An aquaMAX^{TM} (Younglin Instrument, Korea) was used to produce deionized water. All other chemicals and solvents were of analytical grade and used without further purification.

2.2. Fabrication of electrospun nanofibrous mesh

Poly (L-lactide-co-ε-caprolactone) (PLCL) was synthesized by ring-opening polymerization (Mw 439000 g mol^{-1}). In brief, a stannous octoate was homogeneously mixed with L-lactide (LA) and ε-caprolactone (CL) in a glass ampule (LA:CL= 50:50, molar ratio), and purged with nitrogen gas for 12 h. The polymerization was carried out at 150 °C for 24 h with mechanical stirring. After the reaction, the polymer was dissolved in chloroform and then precipitated by dropping into an excess of cold methanol. Finally, the precipitant was dried at 50 °C under vacuum for 72 h. For electrospinning, a 4 wt% PLCL solution was prepared by dissolving in the mixture of dichloromethane and 2, 2, 2-trifluorothanol (8:2, v/v), and the polymer solution was then filled into a plastic syringe (10 mL) equipped with a 21G blunted stainless-steel needle. The syringe was then placed in a syringe pump (KD Scientific single-syringe infusion pump, Holliston, MA, USA), and the solution was ejected to a collector at a distance of 20 cm from the needle tip under 18 kV from a high-voltage power supply (NanoNC, Seoul, Korea). The solution flow rate and spinning time were set to 1 mL h^{-1} and 10 h, respectively. Following the spinning process, the scaffolds were dried at room temperature for 6 h and 40 ºC overnight.

2.3. Acrylic acid (AAc) grafting on PLCL mesh

PLCL meshes were immersed in an aqueous AAc solution (1, 5 and 10% with 0.01 M ammonium ferrous sulfate), and then exposed to a γ-ray irradiation dose rate of 10 kGy h^{-1}. The total dose was 10 kGy at room temperature. After the reaction, unreacted monomers and homopolymer were washed out using DW for several times. The AAc-grafted PLCL meshes were stored in a desiccator after the drying at 40 ºC for further use.

2.4. Scanning electron microscope and water contact angle

The morphology and diameter of meshes were observed using a scanning electron microscope (SEM JSM-6390, JEOL, Tokyo, Japan). For imaging, the meshes were coated with gold using sputter coating for 60 s, and the images were then obtained at an acceleration voltage of 10 keV. The average diameter of the samples was analyzed using an Image J (NIH, MD, USA). Surface wettability was examined by observing the water contact angle on the meshes (Phoenix 300, Surface Electro Optics Co. LTD., Suwon, Korea). All samples were fixed on a glass slide, and 10 μL of water was then dropped onto the meshes. The water contact angle was analyzed by calculating the degree of angle from the captured images using an Image J.

2.5. ATR-FTIR and TBO staining

The surface property of the meshes was analyzed using an attenuated total reflection Fourier transform infrared spectroscopy (ATR-FTIR) spectrophotometer (Bruker TEMSOR 37, Bruker AXS. Inc., Karlsruhe, Germany). The spectra were measured in the region of 500-4000 cm^{-1} at a resolution of 4 cm^{-1} in ATR mode. The introduced carboxylic groups on the meshes were quantified by toluidine blue O (TBO) staining. Briefly, the meshes were incubated in the TBO solution (0.01 M HCl, 20 mg NaCl and 4 mg toluidine blue O chloride) for 4 h at room temperature. The stained samples were vigorously washed several times, and the samples were then re-incubated in a mixture (0.1 M NaOH

and ethanol with 1:4 volume ratio) until the stained TBO was thoroughly released. The uptake amounts of TBO were then quantified by measuring the absorbance at 630 nm using a plate reader (Powerwave XS, Biotek, VT, USA).

2.6. Immobilization of EGF and gelatin on AAc-grafted mesh

The chemical conjugation of EGF (Peprotech, NJ, USA) or gelatin on the AAc-grafted mesh (5 wt% AAc-10 kGy) was conducted by EDC/NHS reaction. Briefly, the meshes were immersed in an MES buffer (pH 5.1) containing EDC/NHS (5 mg mL^{-1}), and incubated for 30 min. The EDC/NHS solution was replaced with EGF solutions (10, 100 and 200 ng mL^{-1}) prepared in a sodium bicarbonate buffer (pH 8.3) or gelatin solution (2 mg mL^{-1}) and then subsequently incubated for 150 min. For co-immobilization of EGF and gelatin, EGF-conjugated mesh (reacted with EGF 200 ng mL^{-1}) was re-activated by EDC/NHS, and then the gelatin solution was sequentially reacted for 150 min. For a control group, same concentration of gelatin was passively adsorbed on the mesh without EDC/NHS reaction. At each conjugation process, unbound EGF or gelatin was completely washed with a sodium bicarbonate buffer and PBS. The modified meshes were stored for one day at 4 °C for further experiments.

2.7. Quantification of immobilized EGF or gelatin

Quantification of conjugated EGF or gelatin was performed with ELISA and fluorescamine assay, respectively. To quantify the amounts of immobilized EGF on the meshes, we indirectly measured the concentration of withdrawal EGF solution after immobilization and re-measured the EGF released from the meshes during washing process. All processes were conducted as recommended by the manufacturer (Peprotech, Rocky Hill, NJ). The immobilized amounts of gelatin were quantified with a fluorescamine assay. The reacted gelatin solution and washed solutions were withdrawn after the reaction. Briefly, a fluorescamine solution (4 mg mL^{-1}, acetone) was mixed in a 0.25 M borate buffer (pH 9) with a mixing ratio of 1:9, which was mixed with the remaining or washed solutions (mixing ratio 25:75). Following the reaction with the fluorescamine, the fluorescent intensity was observed using a plate reader at 390 nm of excitation and 480 nm of emission wavelength (Spectra Max M2e, Molecular Devices, CA, USA). A standard calibration curve was obtained using known concentrations of gelatin (20 - 2000 μg mL^{-1}).

2.8. Viability of hMSCs on the meshes

The meshes were pre-wetted with 70% ethanol and washed several times with PBS. After sterilization under UV light for 60 min, hMSC (passage#6, PT-2501, Lonza Group Ltd., Basel, Switzerland) was seeded on the samples at a density of 3.2×10^3 cells cm^{-1} and cultured for 7 days. At a predetermined point in time, a CCK-8 solution (Dojindo Molecular Technologies Inc., Kumamoto, Japan) was added to the well (medium:CCK = 9:1), and the plates were then kept at 37 ºC for 2 h. Following the incubation, the absorbance of solutions (200 μL) was measured at a wavelength of 450 nm by a plate reader.

2.9. Immunofluorescence staining

We observed the adherent morphology or specific protein expression of the cells (3.2×10^3 cells cm^{-1}) on the meshes using immunofluorescence staining. After 1 or 7 days of culture, the specimens were fixed using 3.7% paraformaldehyde for 15 min and the cells were then permeabilized in a cytoskeletal buffer solution (0.29 g NaCl, 0.5 ml Triton X-100, 0.06 g $MgCl_2$, 10.30 g sucrose, 0.47 g HEPES buffer, in 100 mL water, pH 7.2) for 10 min at 4 °C. After blocking with 1% BSA for 1 h at 37 °C, the fixed cells were incubated with 1:200 rhodamine-phalloidin for 1 h at 37 °C. The cells cultured for 7 days were fixed and blocked as described above, and incubated with anti-involucrin (1: 100, Sigma Aldrich, MO, USA) for 60 min at 37 °C. After PBS washing, the cells were subsequently incubated with 1: 50 Alexa fluor 488 rabbit anti-mouse IgG, 1: 100 rhodamine-phalloidin, and 1: 5000 Hoechst 33258 for 60 min at 37 °C. The specimens were mounted on glass slides with Vectorshield mounting medium (Vector Laboratory, Peterborough, UK). Immunofluorescence images were obtained using a fluorescent microscope (DMI 4000B, Leica, Wetzlar, Germany).

2.10. Quantification of procollagen (type I) secretion

To determine procollagen secretion from the cultured cells on the meshes, we used ELISA kit for procollagen (type I) (Takara Bio Inc., Shiga, Japan). hMSC (1×10^5 cells $well^{-1}$) was cultured on EG-AP meshes with different EGF feed concentrations (10, 100 and 200 ng mL^{-1}). Following 72 h of the incubation, the culture medium (200 μL) was withdrawn and measured the secreted procollagen as instructed by manufacturer.

2.11. Statistical analysis

All data are presented as mean ± standard deviation for n=3. The statistical significance was assessed using one-way ANOVA, Tukey's honest significant difference test and a Student's t-test ($p < 0.05$).

3. Results and Discussion

3.1. Fabrication of AAc-grafted PLCL mesh

ECM-like fibrous scaffolds have been fabricated by an electrospinning technique. Electrospinning is a simple and versatile method for the generation of fibres, whose diameter has been regulated by altering the polymer concentrations or electrospinning condition.[21] In the present study, we used PLCL to develop the nanofibrous meshes. PLCL is a copolymer of lactide and caprolactone synthesized by ring opening polymerization. Its elastomeric property presenting over 500% elongation and 90% recovery has been emphasized

for soft tissue engineering such as heart, vessel, muscle, and skin.[22-25] Surface modification of fibrous meshes has been utilized to modulate the physicochemical property or to induce reactive groups for biomolecules.[26, 27] Graft polymerization of AAc on the substrates is initiated by radical formation. Under AAc solution, the surface of substrate has been active (free radical formation) by γ-ray irradiation, simultaneously vinyl group of AAc is grafted onto the surface. Furthermore, graft density and chain length are determined during this process.[28]

After AAc grafting, we observed the alteration of a fibrous network. PLCL mesh presented a random distribution of each fiber (Fig. 2a), and its fibre diameter was 768.8 ± 117.6 nm. After AAc grafting, we found an increase of fibre diameter up to 874.4 ± 178.5 nm (10% AAc), which was supposed that higher amount of AAc could cover the entire surface of the fibre generating an AAc layer (Fig. 2b). However, the differences in the fibre diameter among the groups were not significant, statistically. Interestingly, the AAc-grafted meshes partially presented winding fibres, in which the degree of winding seems to be increased in an AAc concentration dependent manner. This could indicate that the graft yield was critically affected by the AAc concentration at a constant irradiation dose, and the AAc grafted fibres were swollen in an aqueous condition and then shrunk during the drying process under ambient conditions.[29]

3.2. Characterization of AAc-grafted meshes

After AAc grafting, surface wettability of the meshes was investigated by measuring the water contact angle. Previously, we reported the alteration of hydrophilicity of the fibrous mesh by AAc grafting and RGD peptide conjugation.[30] Hydrophobic feature of the PLCL mesh was changed to hydrophilic owing to the grafted AAc. In the present study, PLCL mesh showed a 75.3 ± 0.7 water contact angle, which was decreased to 60.5 ± 1.9, 42.7 ± 4.3, and 35.4 ± 5.1 degrees according to the reacted AAc concentration of 1, 5, and 10%, respectively. Consistent with the morphology change after swelling and drying, the grafted AAc amounts were regulated by the reacted AAc concentration at a constant irradiation dose, resulting in AAc concentration dependent hydrophilicity increase (Fig. 3a).

How many carboxyl groups were introduced was quantified by TBO staining. TBO staining has been popularly used to measure the induced carboxyl or sulfur group on the materials. It can visualize or quantify the induced amounts of these reactive groups, simply.[31] Whereas non-modified PLCL mesh only presented small amounts of TBO (0.04 ± 0.01 mM), its amount was significantly increased up to 0.1 ± 0.03, 0.6 ± 0.1 and 1.3 ± 0.3 mM, as shown in Fig. 3b. Consistent with previous reports and the above results, the induced AAc amounts were increased in an AAc concentration dependent manner, and in particular, 10% AAc reacted group exhibited a higher carboxyl group content. However, considering the alteration of nanofibre morphology, we chose 5% AAc reacted mesh for further experiments.

3.3. Immobilization of EGF and gelatin

Synthetic polymer-based nanofibrous meshes have been actively modified or mixed with biomolecules for improving the cellular behaviors.[32] For example, a gelatin-PLLA nanofiber successfully promoted the adhesion or proliferation of human microvascular endothelial cells.[33] VEGF and platelet-derived growth factor (PDGF) conjugated multi-layered small-diameter vascular scaffolds also improved the endothelialization and inhibited smooth muscle hyper proliferation.[34] From these reports, the importance of biomolecules has been addressed for tissue engineering. Among the biomolecules that can affect the cellular behaviors, we coupled EGF and gelatin on the AAc-grafted mesh (5% AAc-10 kGy), sequentially.[29,35]

The surface property of meshes was investigated by an ATR-FTIR analysis after conjugation. As shown in Fig. 4, PLCL and AAc-grafted PLCL (AP) meshes showed a representative peak at 1740 cm^{-1} for an ester bond, in which the peak from AP mesh was partially broaden due to the overlapping of C=O stretch from the grafted AAc at 1700 cm^{-1}. As EGF (E-AP) or gelatin (G-AP) was coupled to the AP mesh, new peaks for the amine group and amide bond appeared at 3300 cm^{-1} (N-H stretch) and 1560 cm^{-1} (N-H bend in amide). As gelatin was further coupled to the E-AP mesh (EG-AP), the intensity for the amine group was significantly increased. The major components for amide bond were clearly detected at 1640 cm^{-1} (C=O stretch in amide) and 1560 cm^{-1} (N-H bend in amide). However, we did not find a significant signal for EGF from the EG-AP mesh. It was supposed that the relatively higher amount of gelatin (2 mg mL^{-1}) on the mesh than EGF (200 ng mL^{-1}) might hide the representative signal from the EGF. Moreover, the representative signal from gelatin was not detected from the G-passive mesh. Passively adsorbed gelatin might be removed from the surface during the washing process, and we found that EGF and gelatin chemically immobilized on the meshes.

Quantification of immobilized EGF or gelatin was determined by ELISA or fluorescamine assay. For ELISA, the EGF concentration of withdrawal after the conjugation was indirectly measured. Sodium bicarbonate buffer (for conjugating) and PBS (for washing) were also used for detecting the released or unbound EGF from the surface, in which no EGF was determined from the third washing solution. The coupled amounts of EGF were varied from 8.3 ± 1.6, 72.7 ± 17.1, and 171.7 ± 33.4 ng mg^{-1} mesh, according to the EGF concentrations (10, 100, and 200 ng mL^{-1}) (Fig. 5). The coupling yield reached about 80%, which may be governed by higher carboxyl content induced by γ-ray irradiation. We also used similar procedure for gelatin quantification. Upon the fluorescamine assay, the immobilized gelatin amount was 67.2 ± 30.5 μg mg^{-1} mesh (G-AP), which might be enough for regulating cell responses as described.[29]

3.4. Human mesenchymal stem cell spreading and viability

To investigate the effect of immobilized molecules to the cell spreading and proliferation, we seeded hMSC and cultured for

7 days. It is known that both EGF and gelatin can improve the cell proliferation through EGF-EGF receptor binding or the presentation of collagen-like features, respectively. As EGF was immobilized on the mesh, initial adhesion of hMSC was increased in all E-AP meshes (Fig. 6a). It was approximately 120% higher than that on the PLCL mesh, and this cell adhesion event maintained for further 4 days. However, the enhanced viability after 7 days was not statistically significant in all groups, assuming that the bioactivity of the immobilized EGF maintained until 7 days. G-AP mesh exhibited significantly higher cell viability for 7 days (Fig. 6b). During the culture time, the improvement of cell viability in all G-AP meshes was over 150%. Especially, G-AP mesh (reacted with gelatin 2000 μg mL^{-1}) reached approximately 190%, indicating that gelatin is more powerful in improving cell viability than EGF and its effect retained over 7 days.

After 1 day of culture, we observed the adherent morphology of the cells on the meshes. Previously, PLCL only exhibited low cell adhesion capability owing to the hydrophobicity and absence of cell-interacting cues.[30-31] The adherent cells on the PLCL substrate presented as a spherical shape without filopodia or immature F-actin stress fibers. Although our PLCL mesh also showed similar cell adherent morphology (data not shown), the modified meshes presented a different adherent morphology. In an E-AP mesh, even though we did not find mature F-actin stress fibers or filopodia, the cells altered their morphology partially, spreading into a wider area than those in the PLCL mesh. The spreading area of the cells was significantly increased on the G-AP and EG-AP mesh, in which we found a polygonally spread morphology in a random direction and a mature F-actin stress fibre and filopodia. However, the spreading area of adherent cell was not significantly increased on EG-AP than that from G-AP, indicating that immobilized gelatin may be dominant in regulating cell spreading (Fig. 6c).

The function of EG-AP mesh for cell viability was investigated by comparing with E-AP (EGF in feed 200 ng mL^{-1}) and G-AP mesh (gelatin in feed 2000 μg mL^{-1}). The initial cell adhesion was restricted on the PLCL mesh resulting in poor cell viability, whereas the modified meshes exhibited remarkable improvement of the cell adhesion and viability for 7 days. As shown in Fig. 6d, initial cell viability was increased on EG-AP mesh, and it was 1.4- and 1.2-times higher than that from E-AP and G-AP, respectively. Even though the immobilized molecules did not promote the proliferation rate, this event prolonged for further 7 days of incubation. We found that the co-immobilized EGF and gelatin increased the cell viability. The effect of conjugated biomolecules for cell behaviours was reported by Radisic et al.[36] They prepared VEGF and angiopoietin-1 immobilized scaffolds and described the synergistic effect of co-immobilized VEGF and angiopoietic-1 to the cell proliferation and vascularization. Similarly, we found an effect of co-immobilized EGF and gelatin in cell adhesion and viability, and sequentially immobilized molecules seem to have their own intrinsic roles without any hindrance.

3.5. Immunofluorescence staining for involucrin

Collagen is an abundant protein in various connective tissues in animals, and is found in the skin, muscle, bone, and so on. It has acted a structural platform for cell binding in the ECM, and presented RGD peptide for integrin binding. Similar with collagen, gelatin is a hydrolyzed form from collagen through an acid or base treatment. Although their structures are considerably different, gelatin successfully improves cell adhesion and proliferation similar to collagen. Therefore, a gelatin-coupled nanofiber may act as collagen existing in the ECM, structurally and functionally. EGF involves a general cell proliferation as well as wound repair, and is known to trigger a fast reconstruction of damaged skin tissue and late differentiation.[37] Collectively, because the above distinguishable features may partially mimic the skin construction for skin regeneration, we further investigated whether it can involve the skin regeneration by staining involucrin. Involucrin is a protein component in human keratinocytes. It is present as a soluble protein in the initial state, and then takes part in the formation of a cell envelope. Furthermore, because it is known that its expression has been regulated by EGF treatment,[38] we chose involucrin as a representative marker for skin differentiation.

After 7 days of normal culture without any supplements, the cells on the meshes expressed the involucrin (Fig. 7a). The involucrin revealed in all groups that its expression level was considerably different. The involucrin-stained area in the entire surface (five images were obtained per sample, n=3) was increased in the EGF coupled groups (E-AP and EG-AP), and it was 1.2- and 1.5-times higher than that in the G-AP mesh (data not shown). Furthermore, as normalized by the total nuclei number, the involucrin stained portion was significantly increased in the E-AP and EG-AP mesh, in which the relative value was approximately 3-times higher than that in the G-AP mesh (Fig. 7b). Therefore, the immobilized EGF on the mesh may trigger the trans-differentiation of hMSC to keratinocytes-like cells. Previously, trans-differentiation of stem cells having different lineage to epithelial lineage was reported. For example, adipose-derived stem cells expressed specific markers for keratinocytes such as cytokeratin 10 or involucrin after the keratinocyte-differentiation medium with EGF.[39] hMSC was transdifferentiated to multiple skin cell types under BMP-4 and EGF treatment.[40] Collectively, most of the reports have been involved with EGF to induce keratinocyte differentiation, and we found that EGF might be an essential modulator to the transdifferentiation of a stem cell. Therefore, we can conclude that the immobilized EGF on the mesh may affect the trans-differentiation of hMSC to keratinocyte-like cells.

3.6. Procollagen (type I) secretion

Protein production of cells on materials has been regulated by surface biological property.[41] For instance, FGF basic mixed PLGA nanofiber promoted collagen or tenascin-C synthesis of mesenchymal precursor cells, and described the usage of the

materials for tendon/ligament tissue engineering.[42] In this report, and we explored the protein synthesis involving EGF. Previous literatures describe that EGF itself does not involve the collagen gene expression. However, it has been known to participate to the collagen production by stimulating cell proliferation or involves collagen secretion.[43-44] We investigated its effect to procollagen (type I) secretion (Fig. 7c). Soluble EGF stimulated the procollagen secretion (932.6 ± 81.5 ng mL^{-1}), whereas growth media contains 347.0 ± 63.7 ng mL^{-1}). The secreted procollagen from the cultured cells on the EG-AP meshes with different EGF feed concentrations (10, 100, and 200 ng mL^{-1}) were 657.3 ± 100.9, 740.4 ± 63.7, and 882.9 ± 71.4 ng mL^{-1}, respectively. Although it is difficult to compare the values from soluble EGF and EG-AP meshes directly, we found that the immobilized EGF on the mesh maintained their biological function, and it may promote the procollagen secretion.

4. Conclusions

In the present report, we developed functional fibrous mesh immobilized with EGF and gelatin. The nanofibrous structure of the mesh mimicking the structural feature of native ECM was prepared through an electrospinning method, which was functionalized with EGF and gelatin throughout the AAc grafting by γ-ray irradiation. The modified mesh successfully promoted the spreading and viability of hMSC. In particular, the cultured hMSC on the modified mesh expressed involucrin indicating the trans-differentiation of hMSC to keratinocyte-like cells. Currently, biomimetic scaffolds are attractive for improving the tissue regeneration by reconstructing an artificial ECM microenvironment. As an alternative strategy, co-immobilization of biomolecules to the nanofibrous meshes over two distinct molecules can promote the general cell responses, such as adhesion and proliferation, resulting in outstanding results. Furthermore, the immobilized molecules can exhibit their own function, which can expand the ability of the molecules to the late cell response such as differentiation. Therefore, co-immobilization strategy for developing functional scaffolds may be a good candidate for tissue engineering.

Acknowledgements

This work was supported by National Research Foundation of Korea (NRF) grant funded by the Korea government (MSIP). (2012M2A2A6013196)

Notes and references

[a] Research Division for Industry & Environment, Advanced Radiation Technology Institute, Korea Atomic Energy Research Institute, 29 Gumgugil, Jeongeup 580-185, Korea

[b] Department of Bioengineering, College of Engineering, Hanyang University, 222 Wangsimni-ro, Seongdong-gu, Seoul 133-791, Korea

[*]Corresponding author: Dr. Youn-Mook Lim
Email: ymlim71@kaeri.re.kr
Phone number: +82-63-570-3065
Fax: +82-63-570-3069

[$]These authors equally contributed to this work.

1. H. Shin, S. Jo, A. G. Mikos, *Biomaterials* **2003**, *24*, 4353.
2. H.-W. Kang, Y. Tabata, Y. Ikada, *Biomaterials* **1999**, *20*, 1339.
3. S. I. Jeong, S. H. Kim, Y. H. Kim, Y. Jung, J. H. Kwon, B.-S. Kim, Y. M. Lee, *J. Biomater. Sci., Polym. Ed.* **2004**, *15*, 645.
4. Y. M. Ju, K. Park, J. S. Son, J.-J. Kim, J.-W. Rhie, D. K. Han, *J. Biomed. Mater. Res., Part B* **2008**, *85B*, 252.
5. H. Fernandes, L. Moroni, C. van Blitterswijk, J. de Boer, *J. Mater. Chem.* **2009**, *19*, 5474.
6. C. Frantz, K. M. Stewart, V. M. Weaver, *J. Cell Sci.* **2010**, *123*, 4195.
7. W.-J. Li, C. T. Laurencin, E. J. Caterson, R. S. Tuan, F. K. Ko, *J. Biomed. Mater. Res.* **2002**, *60*, 613.
8. J. A. Matthews, G. E. Wnek, D. G. Simpson, G. L. Bowlin, *Biomacromolecules* **2002**, *3*, 232.
9. M. L. Alves da Silva, A. Martins, A. R. Costa-Pinto, P. Costa, S. Faria, M. Gomes, R. L. Reis, N. M. Neves, *Biomacromolecules* **2010**, *11*, 3228.
10. B. K. Gu, M. S. Kim, C. M. Kang, J.-I. Kim, S. J. Park, C.-H. Kim, *J. Nanosci. Nanotechnol.* **2014**, *14*, 7621.
11. B. K. Gu, S. J. Park, M. S. Kim, C. M. Kang, J.-I. Kim, C.-H. Kim, *Carbohydr. Polym.* **2013**, *97*, 65.
12. M. A. Brady, A. Renzing, T. E. L. Douglas, Q. Liu, S. Wille, M. Parizek, L. Bacakova, A. Kromka, M. Jarosova, G. Godier, P. H. Warnke, *J. Nanosci. Nanotechnol.* **2015**, *15*, 1060.
13. X. M. Mo, C. Y. Xu, M. Kotaki, S. Ramakrishna, *Biomaterials* **2004**, *25*, 1883.
14. A. de Mel, G. Jell, M. M. Stevens, A. M. Seifalian, *Biomacromolecules* **2008**, *9*, 2969.
15. I. Bisson, M. Kosinski, S. Ruault, B. Gupta, J. Hilborn, F. Wurm, P. Frey, *Biomaterials* **2002**, *23*, 3149.
16. S. A. DeLong, J. J. Moon, J. L. West, *Biomaterials* **2005**, *26*, 3227.
17. Y. H. Shen, M. S. Shoichet, M. Radisic, *Acta Biomater.* **2008**, *4*, 477.
18. M. Grellier, P. L. Granja, J.-C. Fricain, S. J. Bidarra, M. Renard, R. Bareille, C. Bourget, J. Amédée, M. A. Barbosa, *Biomaterials* **2009**, *30*, 3271.
19. Y. B. Lee, Y. M. Shin, J.-h. Lee, I. Jun, J. K. Kang, J.-C. Park, H. Shin, *Biomaterials* **2012**, *33*, 8343.
20. T. Stefonek-Puccinelli, K. Masters, *Ann. Biomed. Eng.* **2008**, *36*, 2121.
21. T. J. Sill, H. A. von Recum, *Biomaterials* **2008**, *29*, 1989.
22. K.-Y. Jeong, D.-H. Paik, S.-W. Choi, *Macromol. Mater. Eng.* **2014**, *299*, 1425.
23. J. Jin, S. I. Jeong, Y. M. Shin, K. S. Lim, H. s. Shin, Y. M. Lee, H. C. Koh, K.-S. Kim, *Eur. J. Heart Fail.* **2009**, *11*, 147.
24. I. Jun, S. Jeong, H. Shin, *Biomaterials* **2009**, *30*, 2038.
25. G. Jianying, L. Ninghua, Y. Xinrong, F. Zihao, Q. Fazhi, *Biomed. Mater.* **2014**, *9*, 035012.
26. Y. M. Shin, J.-Y. Lim, J.-S. Park, H.-J. Gwon, S. Jeong, Y.-M. Lim, *Biotechnol. Bioprocess Eng* **2014**, *19*, 118.
27. Z. Ma, W. He, T. Yong, S. Ramakrishna, *Tissue Eng.* **2005**, *11*, 1149.
28. K. Kato, E. Uchida, E.-T. Kang, Y. Uyama, Y. Ikada, *Prog. Polym. Sci.* **2003**, *28*, 209

29. B. Vázquez-González, H. I. Meléndez-Ortiz, L. Díaz-Gómez, C. Alvarez-Lorenzo, A. Concheiro, E. Bucio, *Macromol. Mater. Eng.* **2014**, *299*, 1240.
30. Y. M. Shin, K. S. Kim, Y. M. Lim, Y. C. Nho, H. Shin, *Biomacromolecules* **2008**, *9*, 1772.
31. Y. M. Shin, H. Shin, Y. Lim, *Macromol. Res.* **2010**, *18*, 472.
32. L. Grøndahl, A. Chandler-Temple, M. Trau, *Biomacromolecules* **2005**, *6*, 2197.
33. G. Delaittre, A. M. Greiner, T. Pauloehrl, M. Bastmeyer, C. Barner-Kowollik, *Soft Matter* **2012**, *8*, 7323.
34. M. Moffa, A. Polini, A. G. Sciancalepore, L. Persano, E. Mele, L. G. Passione, G. Potente, D. Pisignano, *Soft Matter* **2013**, *9*, 5529.
35. F. Han, X. Jia, D. Dai, X. Yang, J. Zhao, Y. Zhao, Y. Fan, X. Yuan, *Biomaterials* **2013**, *34*, 7302.
36. J. Berlanga-Acosta, J. Gavilondo-Cowley, P. López-Saura, T. González-López, M. D. Castro-Santana, E. López-Mola, G. Guillén-Nieto, L. Herrera-Martinez, *Int. Wound J.* **2009**, *6*, 331.
37. L. L. Y. Chiu, M. Radisic, *Biomaterials* **2010**, *31*, 226.
38. V. H. Fan, A. Au, K. Tamama, R. Littrell, L. B. Richardson, J. W. Wright, A. Wells, L. G. Griffith, *Stem Cells* **2007**, *25*, 1241.
39. R. Jans, G. Atanasova, M. Jadot, Y. Poumay, *J. Investig. Dermatol.* **2004**, *123*, 564.
40. C. Chavez-Munoz, K. T. Nguyen, W. Xu, S.-J. Hong, T. A. Mustoe, R. D. Galiano, *PLoS ONE* **2013**, *8*, e80587.
41. T.G. Kim, H. Shin, D. W. Lim, *Adv. Func. Mater.* **2012**, *22*, 2446.
42. S. Sahoo, L.-T. Ang, J. C.-H. Goh, S.-L. Toh, *Differentiation* **2010**, *79*, 102
43. M. Laato, V.M. Kähäri, J. Niinikoski and E. Vuorio, *Biochem. J.* **1987**, *247*, 385
44. Y. Mimura, H. Ihn, M. Jinnin, Y. Asano, K. Yamane, K. Tamaki, *Matrix Biol.* **2006**, *25*, 202

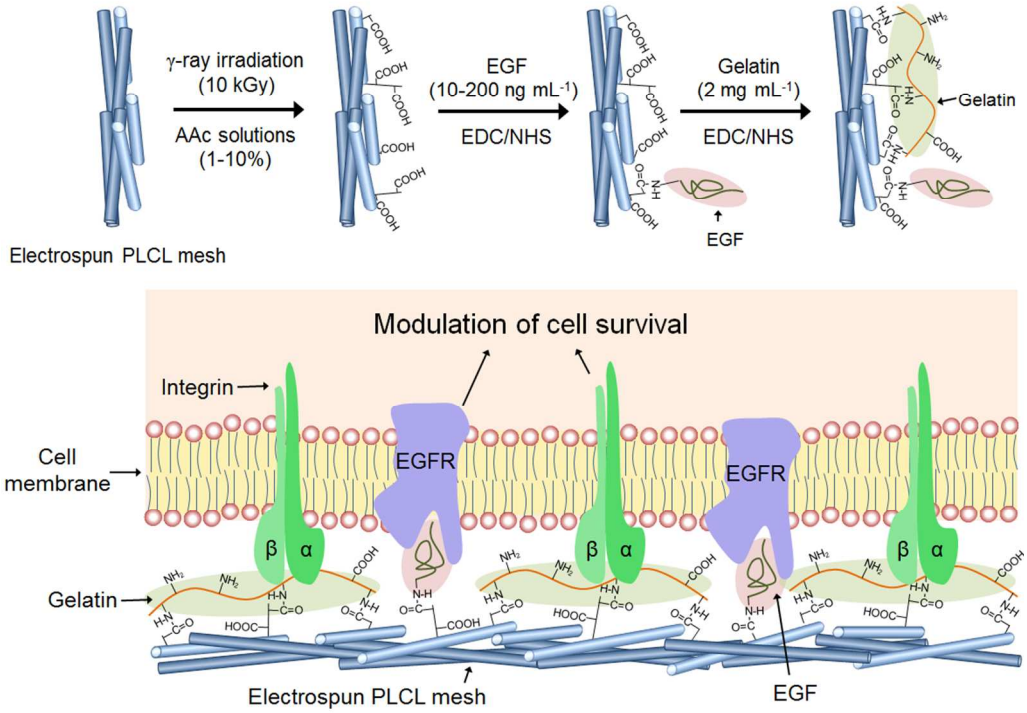

Fig. 1. Schematic diagram of research and illustration for cell adhesion on a fibrous mesh co-immobilized with EGF and gelatin

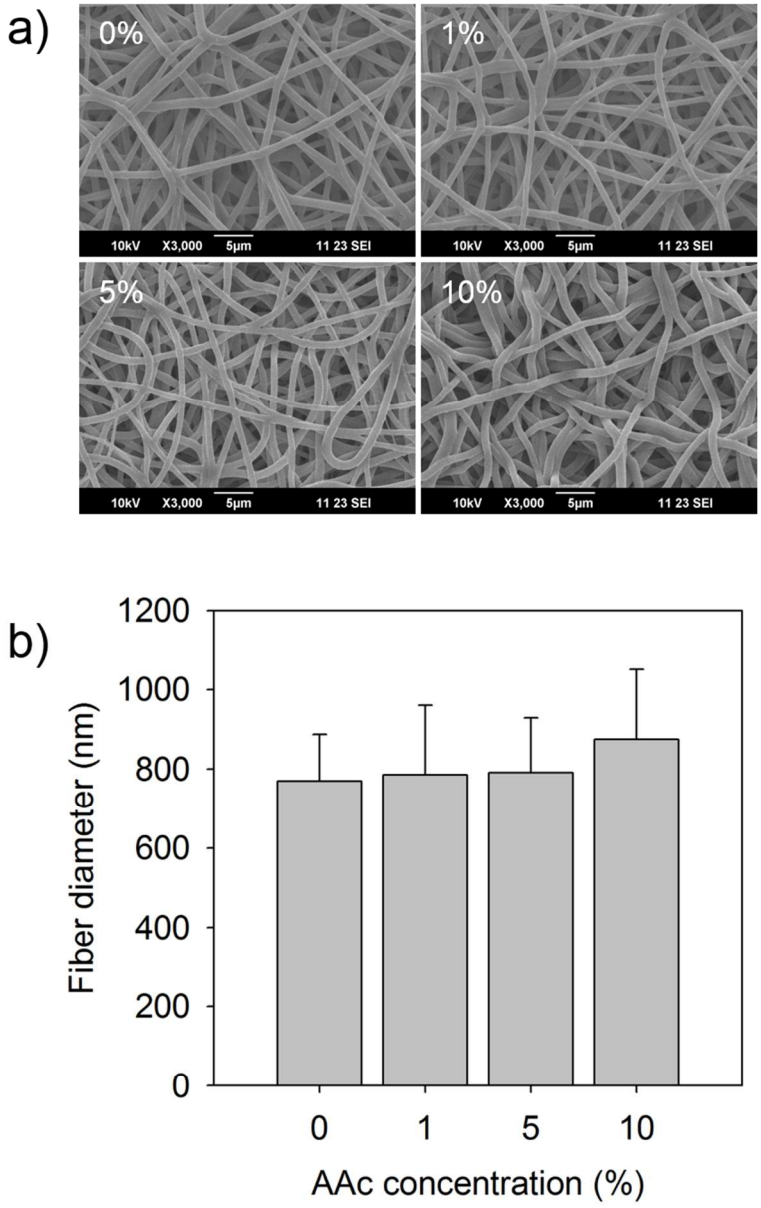

Fig. 2. Morphology of the electrospun fibrous meshes. (a) Scanning electron microscopic images of meshes exposed to various AAc concentrations from 1 to 10% at 10 kGy γ-ray irradiation dose, and (b) mean diameter of the fibres after AAc grafting

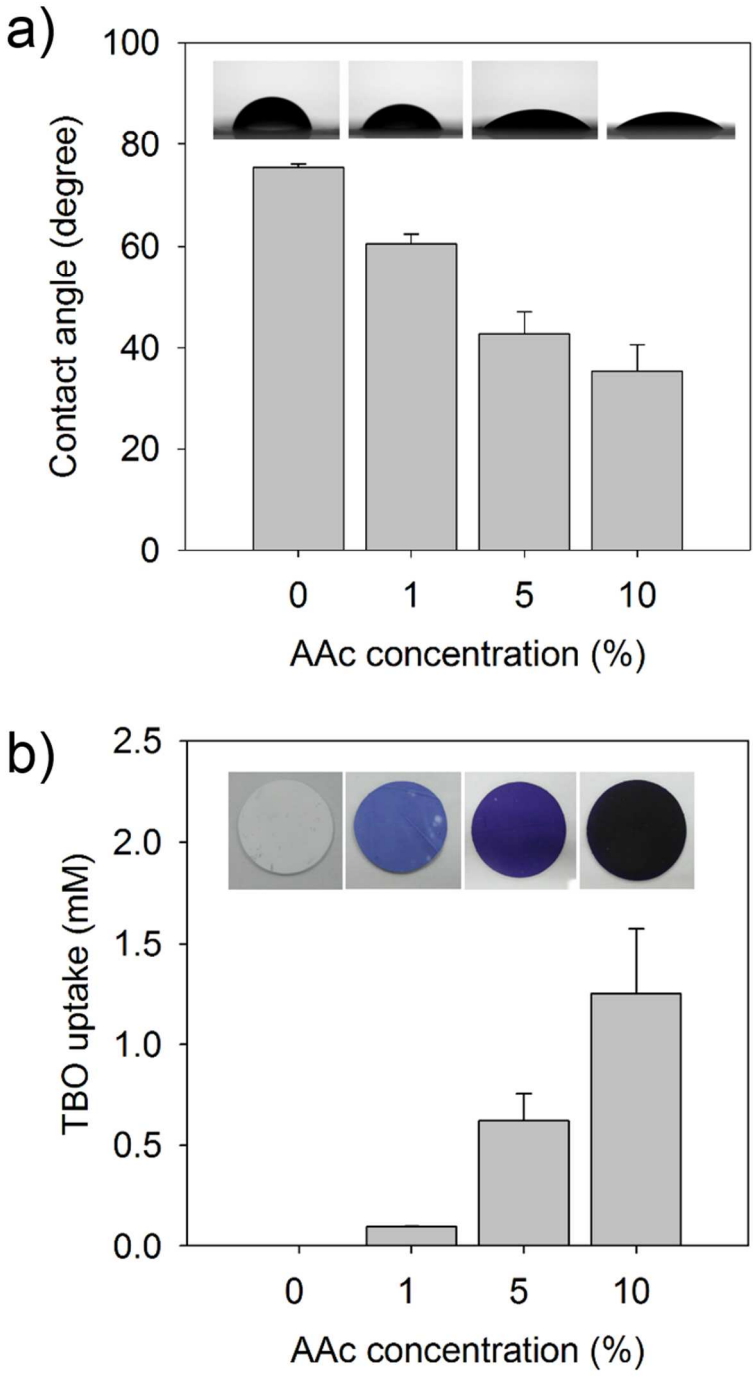

Fig. 3. Characterization of AAc-grafted meshes. (a) Water contact angle measurement (inserted photographs indicate representative water droplet on the meshes) and (b) toluidine blue O uptake for carboxyl group quantification (inserted photographs indicate TBO stained meshes)

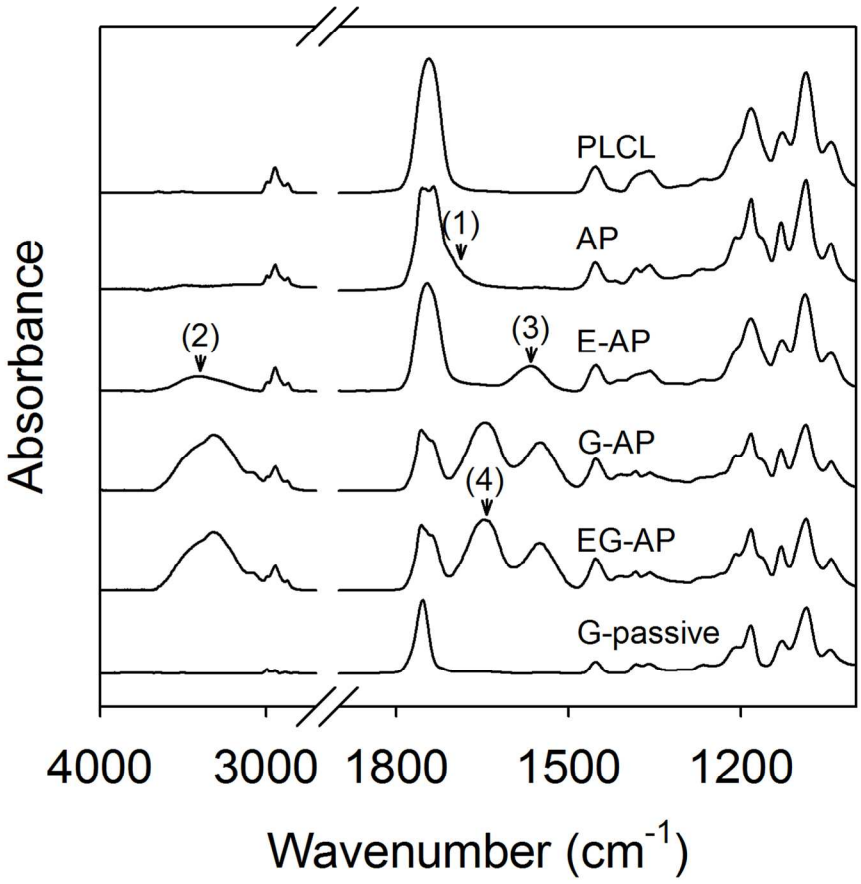

Fig. 4. Surface chemical properties of the meshes. All meshes showed a representative peak at 1740 cm^{-1} for an ester bond, the AP mesh was partially broaden due to the overlapping of C=O stretch from the grafted AAc at (1) 1700 cm^{-1} (C=O stretch) for the carboxyl group. E-AP, G-AP, and EG-AP meshes exhibited new peaks for the amine group and amide bond appeared at (2) 3300 cm^{-1} (N-H stretch), (3) 1560 cm^{-1} (N-H bend in amide), and (4) 1640 cm^{-1} (C=O stretch in amide). In contrast, representative signal from gelatin is not detected on the G-passive mesh.

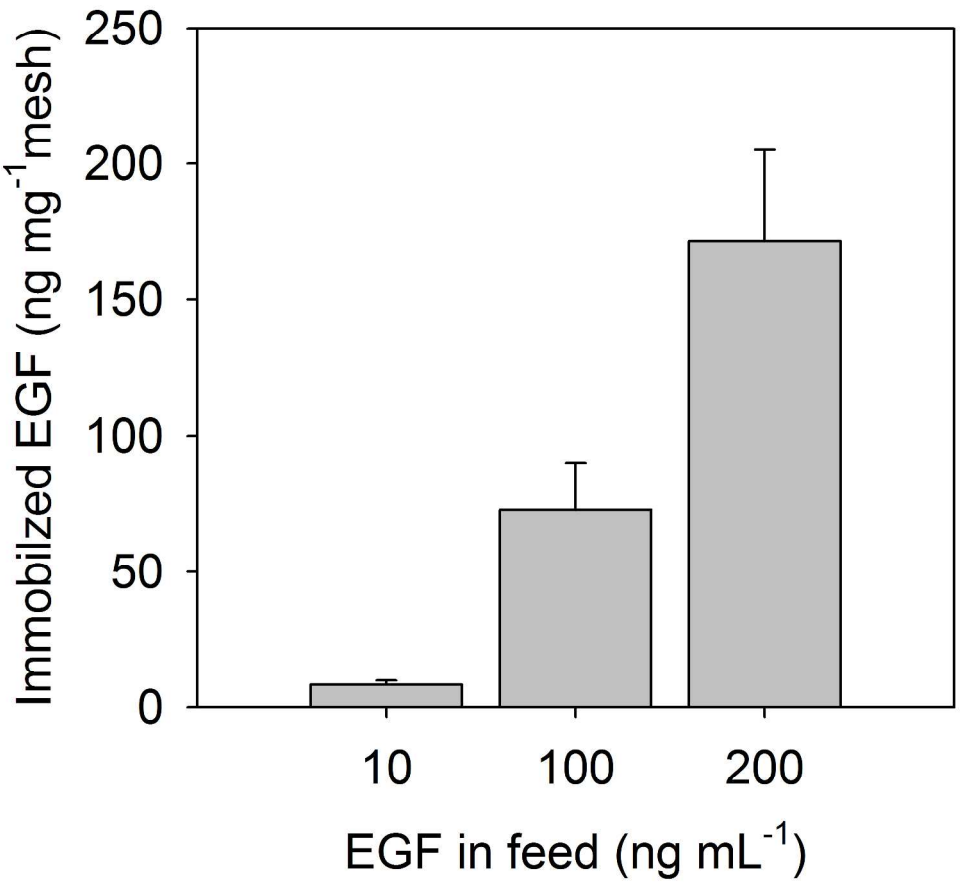

Fig. 5. Quantitative analysis of immobilized EGF on the mesh (2 mg) using ELISA

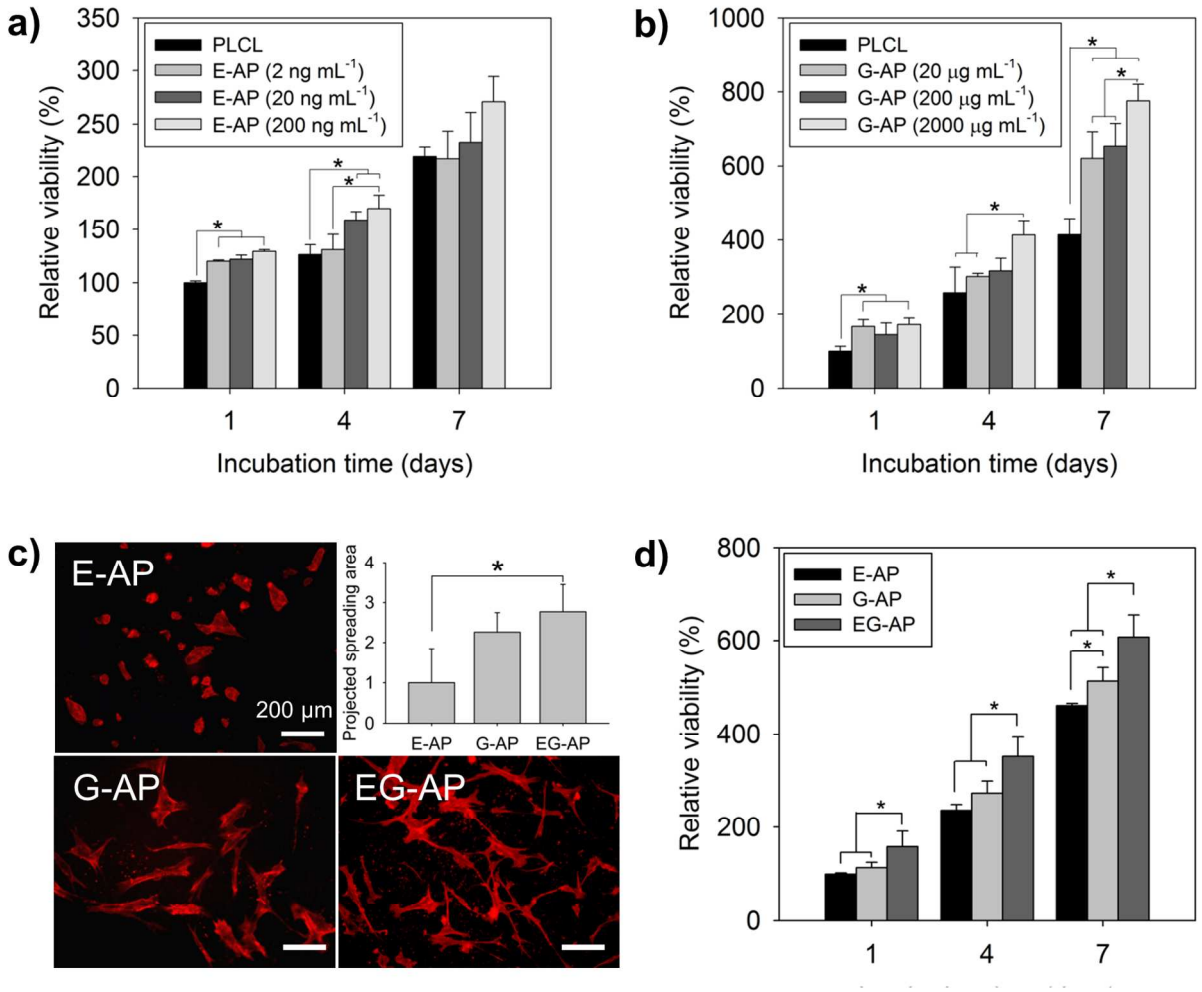

Fig. 6. Viability and spreading of hMSC. (a) relative viability of hMSC on E-AP meshes, (b) relative viability of hMSC on G-AP meshes, (c) spreading of hMSC on the meshes after 24 h of culture (red: F-actin stained by rhodamine-phalloidin), and (d) hMSC viability on the meshes for 7 days. The "*" symbol indicates a significant difference ($p < 0.05$).

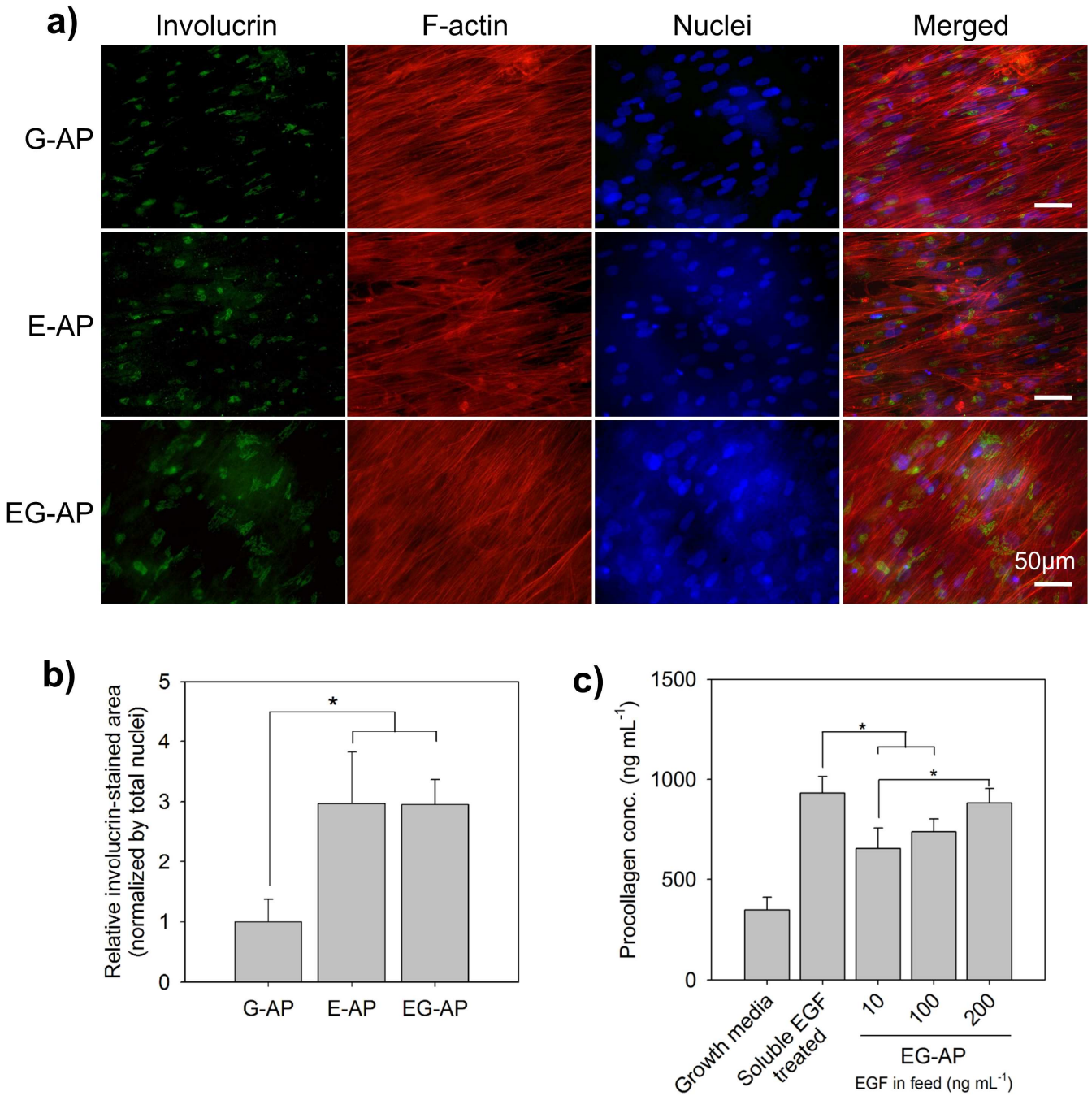

Fig. 7. Involucrin expression of hMSC on the meshes. (a) immunofluorescence images of the hMSC (green: involucrin, red: F-actin, and blue: nuclei), (b) image analysis of involucrin stained area normalized by the total nuclei number (five area per sample, n=3), and (c) quantification of procollagen synthesis by soluble EGF (100 ng mL^{-1}) and immobilized EGF. The "*" symbol indicates a significant difference ($p < 0.05$).

Table of contents

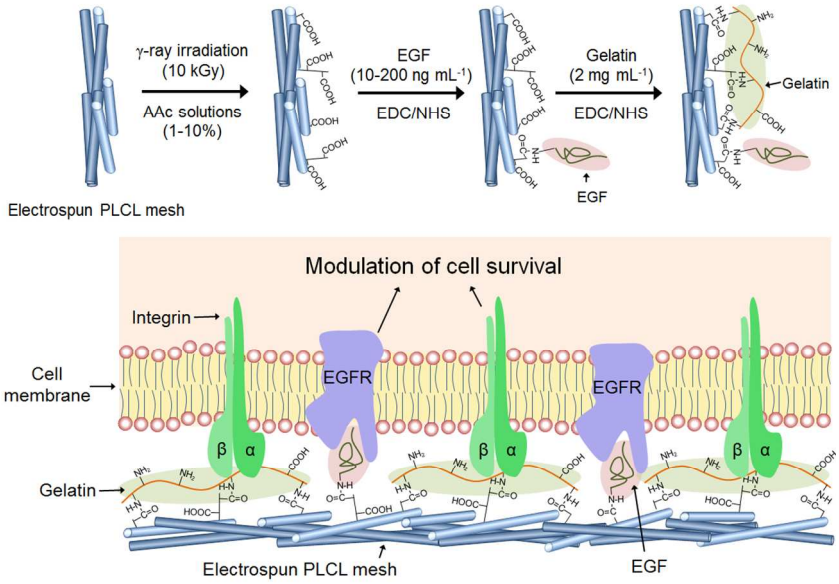

Co-immobilization of EGF and gelatin on a fibrous mesh promotes spreading and viability of hMSC, and coupled EGF involves involucrin expression and procollagen secretion, indicating trans-differentiation to keratinocyte-like cell.